Midinfrared optical absorption in germanium measured with a free-electron laser at room temperature

H. Furuse, N. Mori, H. Kubo, H. Momose, and M. Kondow
Department of Electronic Engineering, Osaka University, Suita City, Osaka 565-0871, Japan
(Received 2 May 2006; revised manuscript received 4 August 2006; published 13 November 2006)

We have investigated the effects of high-power laser pulses on a transparent material using a free-electron laser (FEL). We have measured optical transmittance through a germanium crystal in the midinfrared region, $\lambda = 5.3-12.4$ μm at room temperature. In spite of the fact that germanium is transparent in the midinfrared region, we have observed strong suppression of optical transmission under high-intensity FEL excitation.

DOI: 10.1103/PhysRevB.74.205206 PACS number(s): 78.20.−e, 41.60.Cr, 42.70.Km, 78.30.−j

I. INTRODUCTION

Various nonlinear and nonequilibrium effects in solids have been examined ever since the invention of the laser. In nonlinear and nonequilibrium conditions, electrons in atoms and solids show quite different behavior from those in linear and equilibrium conditions. For example, atoms under high-intensity laser excitation exhibit above-threshold ionization,[1] and high-order harmonic generation.[2] In recent years, the optical dielectric modification of transparent materials induced by use of nonlinear effects with femtosecond laser pulses has been realized.[3] Its application in fabricating photonic devices has received great attention as a new tool of microfabrication. The induction of refractive-index change can be used for the fabrication of waveguides, gratings, and optical memories.[4]

A number of important energies of semiconductors are present between the midinfrared (MIR) and far-infrared (FIR) regions.[5] However, the infrared region is difficult to access experimentally, because of technical restrictions. A free-electron laser (FEL) is suitable for one to research the nonlinear and nonequilibrium effects of crystals in the infrared region. The FEL is a coherent optical source using a relativistic electron beam in a magnetic field as a gain medium. The FEL system consists of a relativistic electron accelerator, an undulator in which the electrons emit the synchrotron radiation, and an optical resonator. By virtue of its simple gain medium, the FEL has unique advantages, the broad wavelength tunability and high-intensity output power. The FEL does not have the restrictions of conventional lasers on operating wavelengths, and will support advanced studies in chemistry, physics, biology, and more in the infrared region.

By using intense pulses of coherent terahertz (THz) radiation from a FEL, THz sideband generation has been studied in $GaAs/Al_xGa_{1-x}As$ quantum wells.[6] In that work, the internal structure and nonlinear response of magnetoexcitons have been probed with intense THz electric fields, and sideband generation due to the THz nonlinear dynamics of confined excitons has been observed. By using intense pulses of MIR radiation from a FEL, band-gap luminescence from a variety of compound semiconductors has also been observed.[7] In that work, an impact ionization model was proposed to explain the FEL-induced band-gap luminescence.

The infrared region is at the transition between the classical and quantum regimes. Zener tunneling is one of the representative phenomena in the limiting case of low frequencies and very strong electric fields. It was originally described in 1934 by Zener:[8] in the presence of a large electric field on a crystal, direct tunneling of a Bloch particle into the continuum of states of another energy band takes place without extra energy. In contrast, multiphoton absorption processes, in which several photons are absorbed simultaneously, are one of the representative phenomena at high frequencies.[9] The transition between these two extremes, is a topic of long-standing theoretical interest,[10,11] but only a few experimental works have previously been published.[12–15] The crossover between "high" and "low" frequency may be quantified in term of the Keldysh parameter γ[10] defined as

$$\gamma = \frac{\omega}{\omega_t} = \frac{\omega (m E_g)^{1/2}}{eF}. \quad (1)$$

Here ω is the frequency of the electric field, $\omega_t = eF/(mE_g)^{1/2}$ is the tunneling frequency, E_g is the band-gap energy, F is the electric field intensity, e is the elementary charge, and m is the electron effective mass. When $\gamma \ll 1$, the direction of the electric field does not change during tunneling. Thus, Zener tunneling corresponds to $\gamma \ll 1$. At higher frequencies, however, there should appear a frequency dependence of the tunneling probability, since the electron does not have time to jump through the barrier within one cycle, and multiphoton effects occur for $\gamma \gg 1$.

In the case of $\gamma \sim 1$, the excitonic dynamical Franz-Keldysh effect (DFKE) was observed by examination of the near-band-gap optical properties of a semiconductor multiple quantum well at $\omega \sim 1$ THz and $F \sim 1-10$ kV/cm by using FIR radiation.[12,13] In that work, however, no induced absorption below the band edge was observed. Large ultrafast induced absorption below the band edge and transparency above the band edge of GaAs due to the DFKE have been observed in recent years.[14,15] In that work, the observed induced absorption occurred only during the presence of an intense MIR pulse; i.e., there was no MIR excitation of carriers across the band gap. The authors concluded that the DFKE is an ultrafast virtual process in which no real carriers are created in the sample.

Most of the previous research in the $\gamma \sim 1$ region has concentrated on III-V semiconductors. What seems to be lacking, however, is work on group-IV materials such as silicon (Si) and germanium (Ge). In particular, studies on Ge are

needed, because Ge has a flat transmittance of about 50% in the MIR region and is widely used for fundamental optical components, such as lenses and beam splitters. In addition, a pulse-picking system is designed using a Ge acousto-optic modulator in which the light path can be transiently diffracted to extract a few micropulses from an entire macropulse.[16] Therefore, it is important to investigate the optical properties of Ge under intense laser fields.

In this paper, we explore the MIR optical properties of a bulk Ge sample driven by intense laser fields. We have measured optical transmittance through Ge in the MIR region, $\lambda = 5.3-12.4$ μm using a FEL. We find that the transmission is strongly suppressed under high-intensity FEL excitation and that the wavelength dependence is weak. To check whether this decrease in the transmittance is due to optical absorption, we measured the transmission and reflection power simultaneously. We then found that it is due to optical absorption, because both transmission and reflection power decrease as the FEL power increases. To analyze the experimental results, we calculated the transmittance of Ge within the Keldysh theory.[10]

The plan of the paper is the following. In Sec. II, we will present a typical FEL output and a schematic diagram of the measurement setup. In Sec. III, we will show the wavelength and irradiation power dependence of the transmission spectrum. We will discuss several possible reasons for strong suppression of the optical transmission. Then we will show the calculated results for the transmittance of Ge within the Keldysh theory. A summary is presented in Sec. IV.

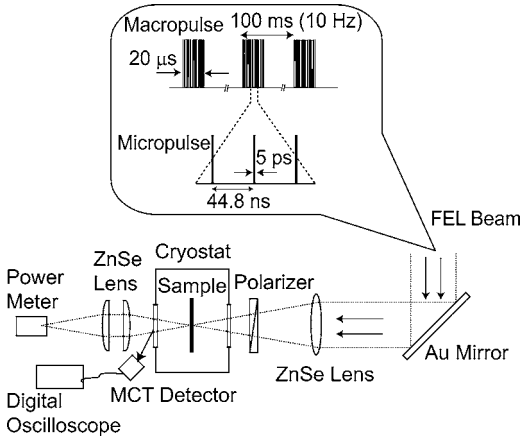

FIG. 1. A typical FEL output and a schematic diagram of the measurement setup. The MIR FEL beam consists of trains of 5 ps pulses (micropulses) with 44.8 ns separation. The train continues for about 20 μs (macropulse) with a repetition rate of 10 Hz. The MIR FEL beam was guided by gold-coated mirrors and focused on a Ge sample by a ZnSe lens of 80 mm in diameter. The sample was put into a cryostat, which has ZnSe windows. A sample holder in the cryostat allows movement in a direction perpendicular to the FEL beam. A polarizer was located between the ZnSe lens and the sample for adjusting the irradiation power. After passing through the cryostat, the transmitted light was focused onto a power meter using two ZnSe lenses. The average power, P_{av}, was measured by the power meter. A portion of the transmitted pulse was recorded with a mercury cadmium telluride (MCT) MIR detector. The MCT output was input to a digital oscilloscope.

II. EXPERIMENTAL METHOD

The experiments were carried out using the FEL facility of the Institute of Free Electron Laser (IFEL), Osaka University at Hirakata, Japan. Figure 1 shows a schematic diagram of a typical FEL output and the measurement setup. The MIR FEL beam consists of trains of 5 ps pulses (micropulses) with 44.8 ns separation. The train continues for about 20 μs (macropulse) with a repetition rate of 10 Hz. We measured optical transmittance through a 3-mm-thick bulk Ge sample in the MIR region $\lambda = 5.3-12.4$ μm at room temperature. The MIR FEL beam was guided by gold-coated mirrors and focused on the Ge sample by a ZnSe lens of 80 mm in diameter. The sample was put into a cryostat, which has ZnSe windows. A sample holder in the cryostat allows movement in a direction perpendicular to the FEL beam. A polarizer was located between the ZnSe lens and the sample for adjusting the irradiation power. We measured the transmitted power with and without a sample. The transmittance was calculated from their ratio. After passing through the cryostat, the transmitted light was focused onto a power meter using two ZnSe lenses. The average power P_{av} was measured by the power meter. Since MIR FEL macropulses suffer from distortion, we measured the temporal variation of the transmission. In order to perform time-resolved transmission experiments, a portion of the transmitted pulse was recorded with a mercury cadmium telluride (MCT) MIR detector, as shown in Fig. 1. The MCT output was input to a digital oscilloscope. We also carried out measurements at a low-power condition using a Fourier transform infrared (FTIR) spectrometer.

Two radio-frequency linear accelerators (rf linacs) with the maximum energy of 165 and 20 MeV are installed at IFEL. The rf linac consists of an injector and linear accelerating waveguides. This type of accelerator has the property that electrons emerge as short bunches, which are separated by fixed periods. Careful synchronization of the circulating micropulses and the electron bunches is required to achieve laser oscillation. However, an electron slips back relative to an optical micropulse on their mutual travel through the undulator, because its velocity is somewhat smaller than the velocity of light and it moves along an undulating path. The slippage distance and the desynchronization between optical pulses and electron bunches give oscillatory structures on FEL macropulse wave forms (see Fig. 2).[17] Moreover, the elongation of the bunch length causes dips in the FEL outputs.[18] The FEL wavelength depends on the kinetic energy of the electron beam (i.e., the electron velocity) and the undulating path. As a result, MIR FEL macropulse structures differ from wavelength to wavelength in these parameters and the FEL resonance conditions.

III. RESULTS AND DISCUSSION

The time-resolved signal and the average power (P_{av}) were used to evaluate the peak power of the incident FEL beam (P_{peak}) and the transmitted beam. First, we measured

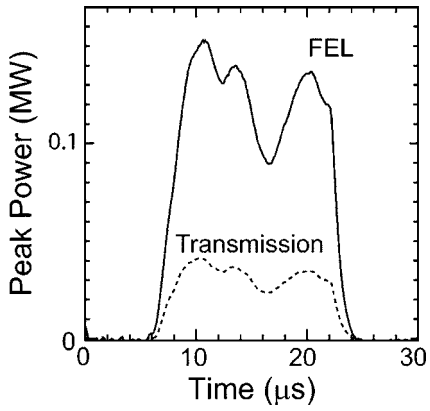

FIG. 2. A typical example of time-resolved signals for the incident FEL beam (solid line) and the transmitted beam (dashed line) for $P_{av}=2.1$ mW and $\lambda=10$ μm.

the average value of the time-resolved signal for 0.1 s (note that the repetition rate of the macropulse is 10 Hz). Second, from the average of the time-resolved signal, we calculated the peak power by considering the measured average power P_{av}, where the micropulse width and interval are set to be 5 ps and 44.8 ns, respectively. In Fig. 2, we plot a typical example of time-resolved signals for the incident FEL beam (solid line) and the transmitted beam (dashed line) for $P_{av}=2.1$ mW and $\lambda=10$ μm. We divided the transmitted signal by the incident FEL signal to obtain the time-resolved transmittance. Since the transmittance at rising and falling edges is unstable, we have neglected the edge parts of the time-resolved signals and adopted the central part between $t\approx 9$ and ≈ 22 μs for the transmittance.

Figure 3 shows the transmittance as a function of the FEL peak power P_{peak} for $\lambda=7$ μm at room temperature. The solid circles represent average values of the peak power and transmittance obtained by time-resolved measurements. The error bars represent the standard deviation of the measurements. In Fig. 3, we also show by the arrow the low-field transmittance measured with FTIR absorption spectroscopy. As can be seen in Fig. 3, the transmittance is strongly suppressed as P_{peak} increases when $P_{peak}<0.1$ MW. For $P_{peak}>0.1$ MW, the transmittance was converged to ~ 0.1. Let us evaluate the γ parameter when $P_{peak}=0.1$ MW from the Keldysh theory of photoionization.[10] The FEL peak power P_{peak} as in Fig. 3 is obtained at the power meter outside the cryostat (see Fig. 1). The transmitted light from the sample passes through a ZnSe window of the cryostat and two ZnSe lenses. By considering the absorption of the ZnSe window and lenses, the peak power at the sample is estimated to be 0.25 MW when the FEL peak power at the power meter, $P_{peak}=0.1$ MW. The electric field strength is then estimated to be $F\sim 1.3$ MV/cm when the beam spot size is 0.06 mm. Thus, γ is evaluated to be ~ 0.8 when $\lambda=7$ μm. Therefore, this regime corresponds to the transition between the classical and quantum regimes. Note that the reduced mass $m=0.034m_0$ and the direct energy gap of Ge, $E_g=0.8$ eV, were used in the above calculation.[19]

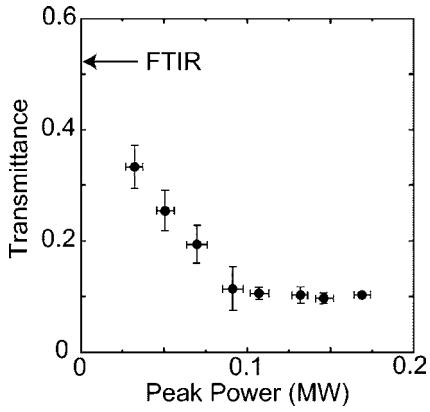

FIG. 3. Transmittance of a 3-mm-thick Ge sample as a function of the FEL peak power P_{peak} for $\lambda=7$ μm at room temperature. The error bars represent the standard deviation of the measurements. Also shown is the low-field transmittance of 0.52 measured with FTIR absorption spectroscopy.

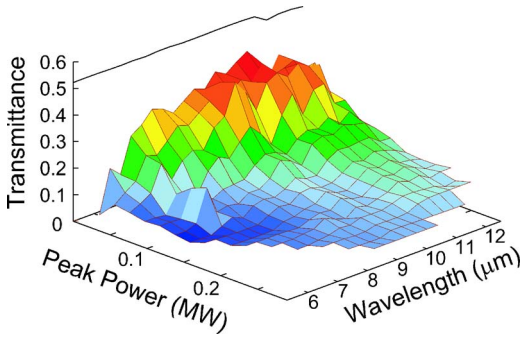

FIG. 4. (Color online). Transmittance of a 3-mm-thick Ge sample as a function of the FEL wavelength λ and the FEL peak power P_{peak} at room temperature. Solid curve shows the transmission spectrum measured by FTIR absorption spectroscopy.

Figure 4 shows P_{peak} dependence of the transmittance for $\lambda=5.3-12.4$ μm at about 0.3 μm intervals. We also plot the transmission spectrum measured by FTIR absorption spectroscopy. As can be seen in Fig. 4, the transmission of the MIR light is strongly suppressed as P_{peak} increases. In addition, we have observed weak wavelength dependence of the transmission spectrum for $\lambda<8$ μm in spite of the fact that the results of the measurements by FTIR absorption spectroscopy do not show the wavelength dependence.

In order to check whether this decrease in the transmittance is due to optical absorption, we measured transmission and reflection power simultaneously. We have to put another power meter close to the sample because the reflection of the MIR light is broad and weak at a point distant from the sample. We tilted the Ge sample so that the power meter is located close to the sample. Figure 5 shows a correlation between $T+R$ and T (T is the transmittance and R is the reflectivity) for various values of the FEL average power P_{av} and the FEL wavelength λ. We find that $T+R$ decreases as T decreases. In Fig. 5, the dashed line shows a theoretical result. The theory assumes an incident angle of 40° in the transmittance and reflectivity measurements. We calculated T and R taking into consideration the absorption coefficient α, where α is changed from zero to infinity. In this calculation, the sample thickness $d=3$ mm and refractive index $n=4$ were used. As can be seen in Fig. 5, there is good agreement

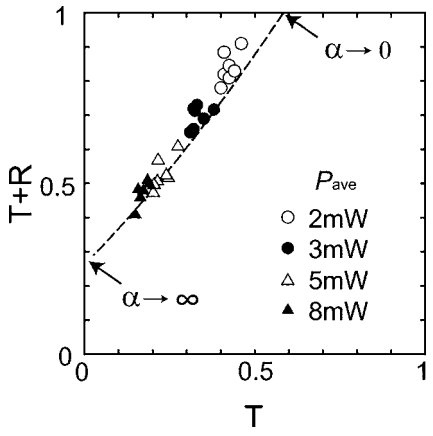

FIG. 5. Correlation between $T+R$ and T for various values of the FEL average power P_{av} and the FEL wavelength λ. Dashed line shows the theoretical result. Note that the theory assumes an incident angle of 40° in the transmittance and reflectivity measurements.

between the theory and the experimental results. Hence, we conclude that the observed decrease in the transmittance is due to optical absorption in Ge.

There are several possible reasons for such absorption below the band edge of the semiconductor. One of the reasons for such absorption is multiphoton absorption (MPA). In Fig. 4, weak wavelength dependence of the transmission spectrum has been observed for $\lambda < 8$ μm. However, the electric field strength increases as λ decreases in the experimental condition when P_{peak} is a constant. By considering this effect, the observed wavelength dependence is found to be much weaker, which cannot be explain in terms of MPA. Another reason for the FEL-induced absorption process is free-carrier absorption. There is a possibility of interband impact ionization induced by residual free carriers accelerated by intense FEL fields. This effect may be able to be checked by studying the temperature dependence of the absorption in Ge. This is under investigation and will be reported in the future.

We find that the absorption does not depend on rotation of the sample in the surface plane, suggesting that the effect is independent on the crystal orientation. Chin *et al.* observed below-band-gap absorption and sideband generation in bulk GaAs using intense picosecond MIR pulses.[14,20] They clearly demonstrated the virtual nature of the effect, that is, no MIR excitation of carriers across the band gap or lattice-heating effects are involved. In this work, however, we find that the observed decrease in the transmittance is due to MIR optical absorption in Ge as shown in Fig. 5. The contribution of the heating effects is considered to be weak, because the time dependence due to heating effects has not been observed. The observed optical absorption may be possible when one take into account of the oscillatory motion of the Bloch electron driven by the intense FEL field when modeling the band-to-band absorption process.[10] To verify this, we have calculated the photoionization probability via the Keldysh theory. Ge is an indirect-gap semiconductor, but the transition usually occurs at the center of the Brillouin zone between the Γ_{4v} valence band and the Γ_{1c} conduction band.[21] Therefore, we have considered direct-gap absorption in Ge.

A detailed derivation of the probability of direct transition from the valence band to the conduction band can be found in Ref. 10, but let us briefly describe it for completeness. The wave function of an electron in an electric field F can be written in the following form:

$$\Psi_{\boldsymbol{k}}^{\alpha}(\boldsymbol{x},t) = u_{\boldsymbol{k}(t)}^{\alpha}(\boldsymbol{x})\exp\left[i\left(\boldsymbol{k}(t)\cdot\boldsymbol{x} - \frac{1}{\hbar}\int_0^t \varepsilon_{\alpha}(\boldsymbol{k}(\tau))d\tau\right)\right],$$

$$\alpha = c, v. \tag{2}$$

Here the indices c and v denote the conduction and valence bands, $\boldsymbol{k}(t)=\boldsymbol{k}+(e\boldsymbol{F}/\hbar\omega)\sin\omega t$, and $\varepsilon_{\alpha}(\boldsymbol{k})$ is the energy of an electron in these bands. $u_{\boldsymbol{k}}^{\alpha}(\boldsymbol{x})$ are periodic functions that have the translational symmetry of the lattice. The probability W_0 of direct transition from the valence band to the conduction band per unit volume is calculated based on first-order time-dependent perturbation theory (i.e., Fermi's golden rule) and can be written as

$$\begin{aligned} W_0 &= \frac{1}{\hbar^2}\lim_{T\to\infty}\mathrm{Re}\sum_{\boldsymbol{k}}\int_0^T dt\langle\Psi_{\boldsymbol{k}}^{c}(\boldsymbol{x},t)|e\boldsymbol{F}\cdot\boldsymbol{x}\cos\omega t|\Psi_{\boldsymbol{k}}^{v}(\boldsymbol{x},t)\rangle \\ &\quad\times\langle\Psi_{\boldsymbol{k}}^{v}(\boldsymbol{x},T)|e\boldsymbol{F}\cdot\boldsymbol{x}\cos\omega T|\Psi_{\boldsymbol{k}}^{c}(\boldsymbol{x},T)\rangle \\ &= \frac{1}{\hbar^2}\lim_{T\to\infty}\mathrm{Re}\sum_{\boldsymbol{k}}\int_0^T L(\boldsymbol{k},t)\cos\omega t\, dt\, L^{*}(\boldsymbol{k},T)\cos\omega T, \end{aligned} \tag{3}$$

where

$$L(\boldsymbol{k},t) = \exp\left\{\frac{i}{\hbar}\int_0^t \varepsilon_{cv}(\boldsymbol{k}(\tau))d\tau\right\}V_{cv}(\boldsymbol{k}(t)), \tag{4}$$

$$V_{cv}(\boldsymbol{k}) = \int u_{\boldsymbol{k}}^{c*}(\boldsymbol{x})e\boldsymbol{F}\cdot\boldsymbol{x}u_{\boldsymbol{k}}^{v}(\boldsymbol{x})d\boldsymbol{x}, \tag{5}$$

and $\varepsilon_{cv}(\boldsymbol{k})=\varepsilon_c(\boldsymbol{k})-\varepsilon_v(\boldsymbol{k})$. We assume that the matrix element V_{cv} varies very slowly as $\boldsymbol{k}$ and is independent of $\boldsymbol{k}$ (this is a good approximation); then V_{cv} may be moved out of the summation. By substituting the Fourier series of Eq. (4),

$$L(\boldsymbol{k},t) = e^{(i/\hbar)\bar{\varepsilon}_{cv}(\boldsymbol{k})t}\sum_{n=-\infty}^{\infty} e^{-in\omega t}L_n(\boldsymbol{k}), \tag{6}$$

into Eq. (3), we obtain

$$W_0 = \frac{2\pi}{\hbar}\left(\frac{eF}{2m\omega}\right)^2 P_{cv}^2\sum_n\sum_{\boldsymbol{k}}|\mathcal{L}_n(\boldsymbol{k})|^2\delta(\bar{\varepsilon}_{cv}(\boldsymbol{k})-n\hbar\omega), \tag{7}$$

where $P_{cv}=(m/eA)V_{cv}$ is the momentum matrix element, A is the magnitude of the vector potential,

$$\bar{\varepsilon}_{cv}(\boldsymbol{k}) = \frac{1}{2\pi}\int_{-\pi}^{\pi}\varepsilon_{cv}(\boldsymbol{k}(\theta/\omega))d\theta, \tag{8}$$

and

$$\mathcal{L}_n(\boldsymbol{k}) = \frac{1}{\pi}\int_{-\pi}^{\pi} \exp\left(i\frac{n}{\bar{\varepsilon}_{cv}(\boldsymbol{k})}\int_0^{\theta} \varepsilon_{cv}(\boldsymbol{k}(\phi/\omega))d\phi \right)\cos\,\theta\, d\theta. \tag{9}$$

Here $\bar{\varepsilon}_{cv}(\boldsymbol{k})$ denotes the average energy gap between valence and conduction bands per cycle in alternating electric fields. In the limiting case of low frequencies and strong fields, these expressions reduce to the formulas for the tunnel effect.[22,23] At high frequencies and low fields, the modified dispersion $\bar{\varepsilon}_{cv}(\boldsymbol{k})$ becomes the unperturbed dispersion $\varepsilon_{cv}(\boldsymbol{k})$, resulting in the relation $W_0 \propto \delta(\varepsilon_{cv}(\boldsymbol{k}) - n\hbar\omega)$ which describes ordinary MPA processes. Therefore, the Keldysh theory comprises a generalization of the theory of tunneling ionization to include multiphoton ionization of crystalline materials in the presence of strong alternating fields.[10]

For the electron energy in the absence of electric field, we assume a simple parabolic band approximation, i.e., $\varepsilon_{cv}(\boldsymbol{k}) = E_g + \hbar^2 k^2/2m$. We used the following parameters in the calculations: $E_g = 0.8$ eV, $m = 0.034 m_0$, and $P_{cv} = 1.36$ a.u.[19,24] The transition probability per unit volume, W_0, was used to evaluate the complex dielectric function $\epsilon_2(\omega)$, which can be expressed as

$$\epsilon_2(\omega) = \frac{2\hbar W_0}{F^2}. \tag{10}$$

The absorption coefficient α then can be expressed as

$$\alpha = \frac{\omega\epsilon_2}{cn}. \tag{11}$$

Here c is the speed of light in vacuum, and n is the refractive index. By neglecting Fabry-Pérot-type interference between surfaces, the transmittance of Ge, T_{Ge}, can be obtained as a function of the sample thickness d by the following equation:

$$T_{\mathrm{Ge}} = \frac{t^2 e^{-\alpha d}}{1 - r^2 e^{-2\alpha d}}, \tag{12}$$

where $r = (1-n)/(1+n)$ and $t = 1 - r$. In the following calculations, we used the refractive index and thickness of Ge as $n = 4$ and $d = 3$ mm, respectively.

In Fig. 6, we show the wavelength dependence of transmittance of Ge calculated using the Keldysh theory at $F = 1.1$ MV/cm. The open circles and solid line represent the calculated results. In Fig. 6, we also plot the experimental results. The solid circles represent the experimental results for $P_{\mathrm{peak}} = 0.2$ MW. These are obtained from Fig. 4. As can be seen in Fig. 6, the calculated results are in reasonable agreement with the experimental results, apart from the oscillatory behavior appearing in the calculated results. Note that the parameter $F = 1.1$ MV/cm was used for the calculation to fit with the experimental results at about $\lambda > 8$ μm. When $\lambda < 7$ μm, the calculated transmittance decreases even further as λ decreases although the experimental transmittance converged to ~0.1. The convergence of the experimental transmittance might be due to laser ablation, since we have often observed laser damage to the surface of Ge when transmittance was less than 0.1.

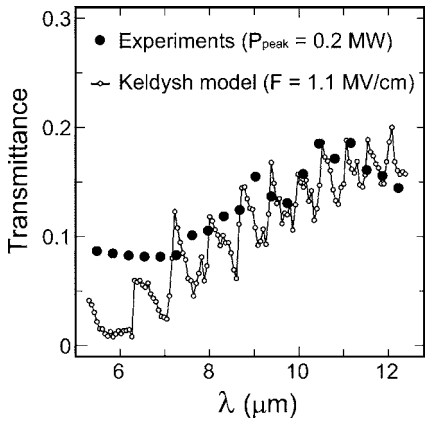

FIG. 6. Transmittance of a 3-mm-thick Ge sample as a function of the wavelength λ, including both theoretical and experimental results. The open circles and solid line represent the calculated results when $F = 1.1$ MV/cm. The solid circles represent the experimental results when $P_{\mathrm{peak}} = 0.2$ MW. There is a reasonable agreement between the theoretical and experimental results, apart from the oscillatory behavior appearing in the calculated results.

IV. SUMMARY

In summary, we investigated the optical transmission in a crystal of the group-IV semiconductor Ge under intense laser fields in the MIR region using a FEL. We observed strong suppression of optical transmission under high-intensity FEL excitation. We find that the decrease in transmission is due to optical absorption below the band edge, i.e., MIR photons are absorbed by electrons in Ge. We also find that the FEL wavelength dependence of the transmission spectrum is weak. The theoretical results using the Keldysh theory are in reasonable agreement with the experimental results.

[1] R. R. Freeman, P. H. Bucksbaum, H. Milchberg, S. Darack, D. Schumacher, and M. E. Geusic, Phys. Rev. Lett. **59**, 1092 (1987).
[2] A. Rundquist, C. G. Durfee, Z. Chang, C. Herne, S. Backus, M. M. Murnane, and H. C. Kapteyn, Science **280**, 1412 (1998).
[3] K. M. Davis, K. Miura, N. Sugimoto, and K. Hirao, Opt. Lett. **21**, 1729 (1996).
[4] K. Yamada, W. Watanabe, J. Nishii, and K. Itoh, J. Appl. Phys. **93**, 1889 (2003).
[5] S. Adachi, J. Appl. Phys. **58**, R1 (1985).
[6] J. Kono, M. Y. Su, T. Inoshita, T. Noda, M. S. Sherwin, S. J. Allen, Jr., and H. Sakaki, Phys. Rev. Lett. **79**, 1758 (1997).
[7] N. Mori, T. Takahashi, T. Kambayashi, H. Kubo, C. Hamaguchi, L. Eaves, C. T. Foxon, A. Patanè, and M. Henini, Physica B **314**, 431 (2002).
[8] C. Zener, Proc. R. Soc. London, Ser. A **145**, 532 (1934).

[9] V. Nathan, A. H. Guenther, and S. S. Mitra, J. Opt. Soc. Am. B **2**, 294 (1985).
[10] L. V. Keldysh, Sov. Phys. JETP **20**, 1307 (1965).
[11] Y. Yacoby, Phys. Rev. **169**, 610 (1968).
[12] K. B. Nordstrom, K. Johnsen, S. J. Allen, A. P. Jauho, B. Birnir, J. Kono, T. Noda, H. Akiyama, and H. Sakaki, Phys. Rev. Lett. **81**, 457 (1998).
[13] A. P. Jauho and K. Johnsen, Phys. Rev. Lett. **76**, 4576 (1996).
[14] A. H. Chin, J. M. Bakker, and J. Kono, Phys. Rev. Lett. **85**, 3293 (2000).
[15] A. Srivastava, R. Srivastava, J. Wang, and J. Kono, Phys. Rev. Lett. **93**, 157401 (2004).
[16] S. Y-Suzuki, T. Kanai, K. Ishii, Y. Naito, and K. Awazu, in *Proceedings of the 26th International FEL Conference and 11th FEL Users Workshop 2004*, edited by R. Bakker, L. Giannessi, M. Marsi, and R. Walker (Comitato Conferenze Elettra, Trieste, Italy), p. 657.
[17] D. A. Jaroszynski, R. J. Bakker, A. F. G. van der Meer, D. Oepts, and P. W. van Amersfoort, Phys. Rev. Lett. **70**, 3412 (1993).
[18] H. Nishiyama, M. Asakawa, Y. Tsunawaki, M. Heya, K. Awazu, and K. Imasaki, Nucl. Instrum. Methods Phys. Res. A **507**, 74 (2003).
[19] O. Madelung, *Semiconductors: Data Handbook*, 3rd ed. (Springer, Berlin, 2004), p. 45.
[20] A. H. Chin, O. G. Calderón, and J. Kono, Phys. Rev. Lett. **86**, 3292 (2001).
[21] P. Y. Yu and M. Cardona, *Fundamentals of Semiconductors*, 2nd ed. (Springer-Verlag, Berlin, 1999).
[22] L. V. Keldysh, Sov. Phys. JETP **6**, 763 (1958).
[23] E. O. Kane, J. Phys. Chem. Solids **12**, 181 (1960).
[24] C. Hamaguchi, *Basic Semiconductor Physics* (Springer-Verlag, Berlin, 2001).